Paper Number: **49**

Title: **In-Situ Observations of Longitudinal Compression Damage in Carbon-Epoxy Cross Ply Laminates Using Fast Synchrotron Radiation Computed Tomography**

Authors: Andrew C. Bergan
Serafina C. Garcea

ABSTRACT

The role of longitudinal compressive failure mechanisms in notched cross-ply laminates is studied experimentally with in-situ synchrotron radiation based computed tomography. Carbon/epoxy specimens loaded monotonically in uniaxial compression exhibited a quasi-stable failure process, which was captured with computed tomography scans recorded continuously with a temporal resolutions of 2.4 s and a spatial resolution of 1.1 μm/voxel. A detailed chronology of the initiation and propagation of longitudinal matrix splitting cracks, in-plane and out-of-plane kink bands, shear-driven fiber failure, delamination, and transverse matrix cracks is provided with a focus on kink bands as the dominant failure mechanism. An automatic segmentation procedure is developed to identify the boundary surfaces of a kink band. The segmentation procedure enables 3-dimensional visualization of the kink band and conveys the orientation, inclination, and spatial variation of the kink band. The kink band inclination and length are examined using the segmented data revealing tunneling and spatial variations not apparent from studying the 2-dimensional section data.

INTRODUCTION

Composite plies in laminates loaded under longitudinal compression often fail by the kink band damage mechanism [1]–[4]. The parameters shown in Figure 1 are often used to describe the kink band: w for the width of the kink band, φ for the fiber misalignment angle, and β for the kink-band inclination angle. Kink bands may develop in the 1-2 plane (in-plane) or in some other plane defined by the angle Ψ. Most observations of kink bands have been made postmortem by examining polished sections with optical or scanning electron microscopy (SEM), e.g. [1]. One drawback of such observations is that the sequence of events is unknown. Gutkin et al. [5] used in-situ scanning electron microscopy SEM to study kink bands in notched unidirectional and cross-ply laminates. Their investigation revealed a mechanism for kink-band initiation

Andrew C Bergan, Structural Mechanics and Concepts Branch, NASA Langley Research Center, Mail Stop 190, Hampton, VA 23681, U.S.A.
Serafina C. Garcea, School of Materials, Henry Moseley X-ray Imaging Facility, University of Manchester, Manchester, M13 9PL, United Kingdom

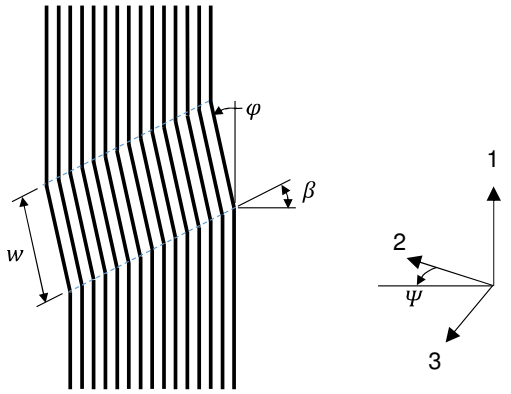

Figure 1. Schematic idealization of a kink band.

referred to as shear-driven fiber compression failure where fibers fail along a 45° shear plane without kinking ($w = 0$). As the fibers slide along the failure surface, shear stresses and fiber bending are induced ahead of the damage, which leads to fiber kinking (w on the order of 5–20 fiber diameters).

While observation under load is an important advance, 2-dimensional (2-D) sectional imaging obscures the 3-dimensional (3-D) features of fiber kinking. X-ray computed tomography (CT) is an alternative approach that allows for nondestructive investigation of fiber kinks in 3-D. Ueda et al. [6] used uniaxial unnotched compression tests to show the non-uniformity of fiber kinking. Wang et al. [7] conducted ex-situ CT scans on interrupted tests of unidirectional specimens loaded under axial compression. The kink-band boundaries and matrix longitudinal splitting damage were segmented and visualized in 3-D. The authors analyzed 2-D images lying in the kink-band plane to measure the characteristics (w, φ, and β) of the kink band. Furthermore, since CT scans are nondestructive, it is possible to perform a sequence of scans at several stage of damage development to examine the evolution of damage. Notched unidirectional specimens loaded in four point bend were found to slow the propagation of kink bands enough to allow for such a time-lapse study of kink bands [8]. The results showed a sequence of fiber damage leading to multiple kink bands. These studies produced important insights into the fiber kinking phenomenon for unidirectional specimens. As of yet, no comparable detailed investigation has been conducted for cross-ply laminates to understand the interaction of kink bands with other damage modes that occur in a laminate, such as delamination.

The objective of this experimental study is to investigate longitudinal compression damage in notched cross-ply laminates. The emphasis of the investigation is on the kink band mechanism since it is thought to dominate the response under longitudinal compressive load. The interaction of kink bands with other damage mechanisms is explored. In order to facilitate a detailed time-lapse study of the fiber kinking process, synchrotron radiation computed tomography (SRCT) to exploit the fast scanning and high resolution capability [9]. The details of the test specimens and in-situ SRCT tests are described in the next section. Subsequently, a chronology of damage events is provided. Finally, an automated segmentation procedure is developed and applied to investigate the morphology of one kink band observed in the test data.

EXPERIMENTAL SETUP

Materials

Specimens were obtained from plates that were fabricated by hand layup of IM7/8552 carbon/epoxy prepreg plies and cured in an autoclave. The specimens were cut from a $[(90/0)_3/90/(0/90)_3]$ laminate with a thickness of 2.15 mm using a waterjet. The notch was machined with a diamond tool and the loading surfaces were ground flat and parallel to the final dimensions shown in Figure 2. The notch length was 6.5 mm. The specimen dimensions were selected to promote stable formation of kink bands while accounting for the constraints of the loading fixture and SRCT system. The relatively slender specimen was stabilized to prevent buckling with fiberglass tabs bonded to the specimen with EA9394 adhesive. In addition, anti-buckling guides were used at the top and at the bottom of the sample along the bonded tabs to prevent any out-of-plane defections. The anti-buckling guides were designed so that there was no interference with the x-ray beam.

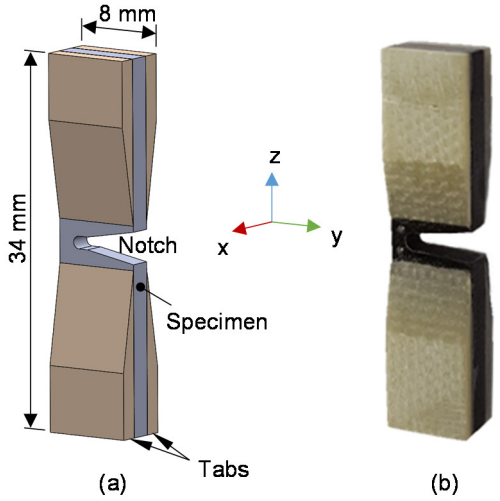

Figure 2. Test specimen configuration: (a) schematic and (b) photograph.

In-Situ SRCT

The experiments were performed on the TOMCAT-X02DA Beamline at the Swiss Light Source, Paul Scherrer Institut, Villigen, Switzerland. Quasi-static compression loading was applied monotonically using a displacement control rate of 1 µm/s with the loading rig provided from INSA-Lyon [9]. Load and actuator displacement were recorded at intervals of 2 Hz.

Incremental interrupted in-situ scans were conducted at 50 N, 250 N, 500 N, and 800 N. After the last incremental scan at 800 N, loading was continued to failure and, at the same time, fast and continuous SRCT scans were recorded with a temporal resolution of 2.4 s. A total of 801 projections were recorded for each scan. The beam (monochromatic) energy used was 20 keV voxel size of 1.1 µm. This setup resulted in a scan volume of about 2 mm x 2 mm x 2 mm in the x, y, and z directions. The scans included the notch tip and ligament ahead of the notch. Reconstructions of the acquired datasets was done in-house using traditional filter back projection (FBP) method with a ring removal algorithm embedded to reduce ring artefacts. In addition, a combination of median and mean filters were applied to reduce noise.

CHRONOLOGY OF DAMAGE DEVELOPMENT

The test specimens exhibited a quasi-stable failure process that allowed for SRCT observations of the damage event chronology, including damage initiation and propagation. This section describes the chronology of damage events for one replicate and the corresponding structural response as a series of five stages.

The load versus cross head displacement response is shown in Figure 3a. After some initial nonlinearity below 250 N, the response is observed to be nearly linear up to 950 N. The peak load was 974 N and the specimen eventually failed at 910 N after some unloading. A zoomed-in view of the load-displacement response near the peak load is shown in Figure 3b. The continuous scanning procedure commenced at 800 N and a total of 40 scans were recorded through the failure process. Through the duration of each scan, the specimen was shortened by 2.4 μm. The scans are overlaid on Figure 3b as white and light gray bars labeled 1–40 to show relation between each scan and the load history.

The damage development process is divided into five chronological stages for the purpose of discussion. The stages are summarized in Table I and overlaid on the load-displacement response in Figure 3b. Stage 0 denotes the relatively minor matrix damage that preceded the formation of kink bands. Although most of the matrix splits occurred before the continuous scanning, some splits grew during stage 0. Growth of matrix splits in 0° plies during stage 0 corresponded with a small load drop of 10 N, circled in orange in Figure 3b. In stage I, kink bands initiated in two of the 0° plies. During stage II, the kink bands that initiated in stage I propagated, which led to a drop in load of about 50 N. In stage III, kink bands formed in the remaining 0° plies. Finally, in stage IV, the kink bands linked together via matrix compressive damage in the 90° plies, which resulted in structural collapse. Each stage of the failure process is discussed in detail in the following sub-sections. Kink bands are designated K_n where $n = 1, 2, 3, \ldots$ corresponds to the 0° ply in which the kink band occurs. Representative images of the damage events observed in each stage are shown and discussed in the following subsections.

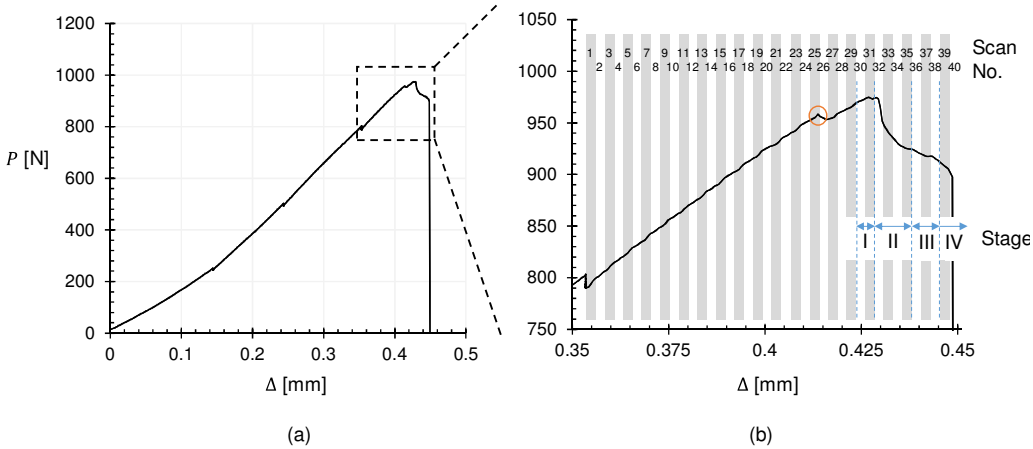

Figure 3. Load-displacement response for the (a) full load history and (b) a zoomed in view of the loading regime recorded by continuous SRCT scanning.

TABLE I. STAGES OF THE FAILURE PROCESS.

Stage	Scans	Description
0	≤ 29	Condition prior to fiber kinking; stable matrix splitting
I	30 – 31	Fiber kinking initiation
II	32 – 35	Propagation of initial kink bands
III	36 – 38	Development of kink bands in all 0° plies
IV	39, 40	Final failure; link-up of damage through-the-thickness

Stage 0: Condition Prior to Fiber Kinking

Matrix damage initiated in the form of longitudinal splitting cracks in the 0° plies after the 500 N scan, and propagated relatively slowly and stably as load was increased through stage 0, up to 970 N. Representative splitting cracks in two orthogonal slice planes near the end of stage 0 are shown in Figure 4. A top view is shown in Figure 4a where the normal to the slice is in the loading direction, z. The notch boundary is located near the top of the image. The slicing plane is shown in parts b and c of the figure to help orient the reader. Matrix splitting cracks are observed in four of the 0° plies as indicated with the white arrows.

A planar view of one representative matrix split in ply 0_4 is shown in Figure 4b, where designation 0_n specifies the location of the 0° ply in laminate with $n = 1, 2, \ldots, 6$ and $n = 1$ closest to $x = 0$. The splits that developed in stage 0 all initiated from the same point on the notch tip, marked with an orange arrow in the figure. The matrix splits initiated from this particular point along the notch front apparently because this point is the apex of the notch length and the irregular notch shape introduce some stress concentration at this location. Though a round notch tip was planned, complications with the machining process due to the high precision required for the relatively small dimensions of the test articles resulted in the meandering notch boundary observed in Figure 4b. The length of the split in this slice is 409 um. The split shows small ligaments bridging the crack (e.g., white arrow in the figure), which are characteristic of Mode II shearing cracks. It is noted that fiber misalignment with a magnitude of about 3° is evident in Figure 4b. Fiber misalignments occurred throughout all plies with a magnitude and direction appearing in clusters separated by resin rich regions, which is consistent with results reported in a detailed study of fiber positions by Fast et al. [10].

One instance of fiber damage was observed to occur in ply 0_5 between the 500 N and 800 N scans. This fiber damage include only a few fibers, as shown in Figure 5, and did not propagate during the stage 0 continuous scans 1–29. The fibers failed in a mode that resembles the shear-driven fiber failure identified by Gutkin et al [5]. It was unexpected that such a failure would occur with no subsequent propagation at a load level well below subsequent fiber failures. The shear-driven fiber failure may have occurred as a result of the fact that these fibers were particularly well aligned at the notch apex and thus subjected to large axial compressive stresses. Alternatively, these premature failures could be a result of a local manufacturing imperfection or machining induced damage in these fibers. Though a kink band did eventually initiate ahead of this shear-driven fiber failure, it did not occur until stage III.

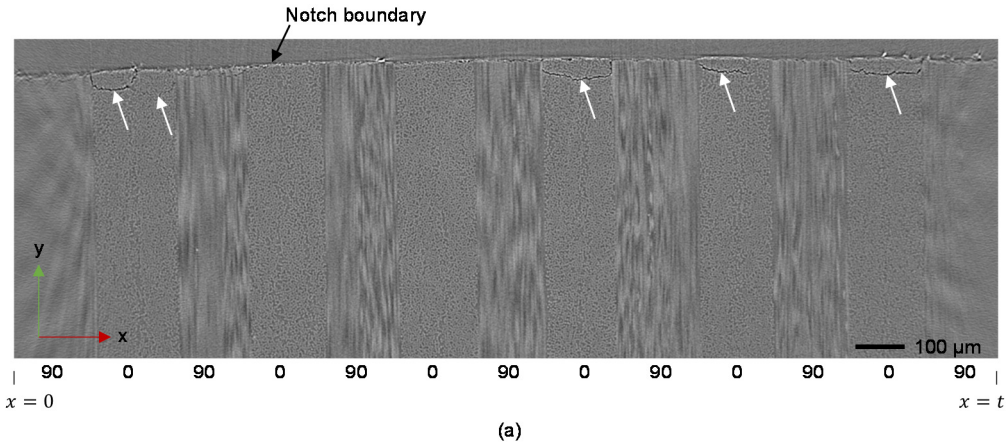

Figure 4. Representative matrix splits that developed during stage 0 where (a) shows section A-A, (b) shows section B-B, and (c) shows schematically the location of the section views.

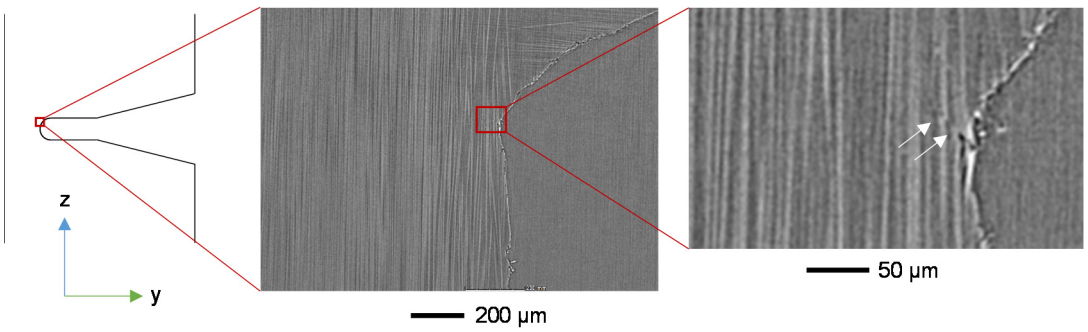

Figure 5. Planar view showing apparent shear-driven fiber failure in ply 0_5 that appeared in the 800 N scan and did not propagate until stage III.

Stage I: Kink Band Initiation

Two kink bands initiated during stage I. First, in the ply 0_1, a kink band designated K_1 was observed in scan 30, as shown in Figure 6. The kink band initiated near the apex of the notch. Planar sections of K_1 shown in Figure 6a show, from left to right, the interface with the outermost 90° ply, two intermediate locations through the thickness of ply 0_1, and the interface with the next 90° ply. The laminate stacking sequences are shown in the figure with the current ply underlined and the nearest interface indicated by a red slash (these conventions are used throughout). The slices at the ply interfaces show that the kink is accompanied by delaminations (orange arrows). The length of the kink in the y-direction is $\cong 330$ μm. It is also observed that w_{KB} increases from nearly zero at the notch tip (white arrow in Figure 6a) to $w_{\mathrm{KB}} \cong 5d$ at the farthest sections from the notch tip, where $d = 7$ μm is the fiber diameter. Apparently, near the notch tip where $w_{\mathrm{KB}} \cong 0$ the failure mode was shear-driven fiber failure. Cross-sections with a y-direction normal are shown in Figure 6b for several locations measured from the notch tip. The distance in μm from the notch tip to the section plane is labeled in white in the upper right corner of each image in Figure 6b. The delaminations observed in Figure 6a are marked with orange arrows. The images in Figure 6b show that K_1 is an out-of-plane kink and that the delaminations are consistent with the out-of-plane fiber rotations in the kink band. Matrix splitting cracks (white arrows) accompany fibers that exhibit large bending. In sections located farther from the notch tip (378 μm, 406 μm, and 427 μm) it is observed that the kink band does not extend through the thickness of the ply.

In the next scan, 31, a second kink, K_2, was observed in the adjacent 0° ply, 0_2. A series of four planar section views through the thickness of ply 0_2 are shown in Figure 7. K_2 initiated in the same location with respect to the notch as K_1. Though referred to as a kink band, nearly all of the damage fibers appear to have failed by the shear-driven

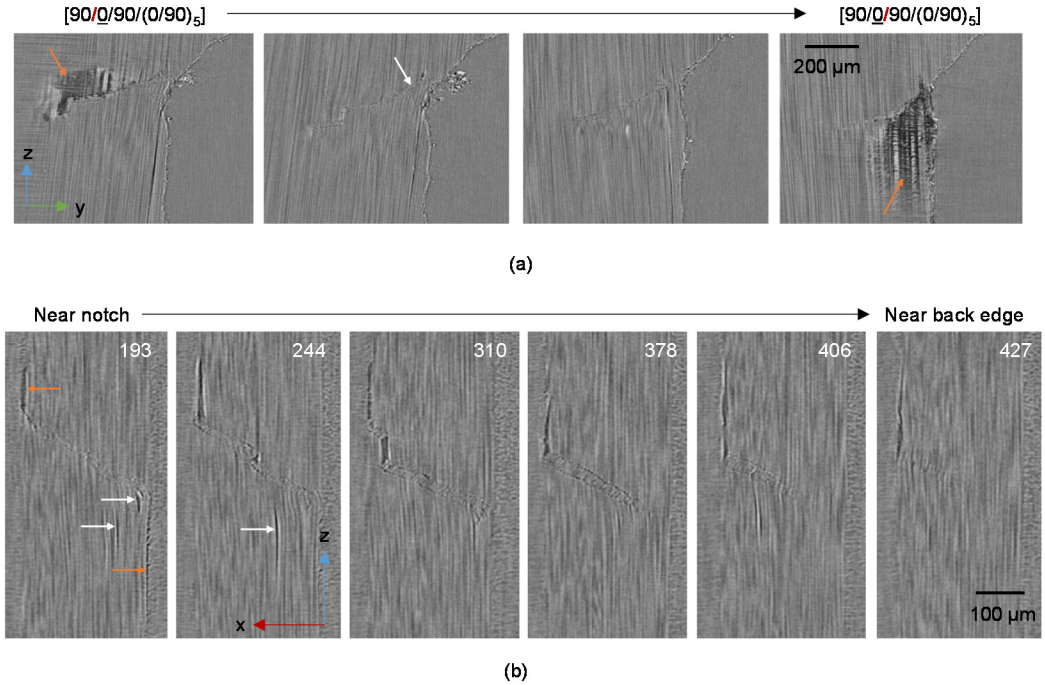

Figure 6. Images of the first fiber kinking event, ply 0_1, scan 30.

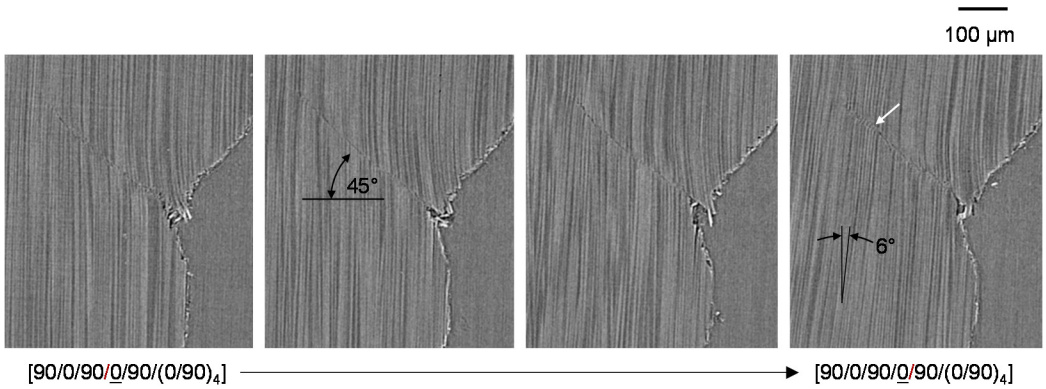

Figure 7. Planar sections of the second kink band, K_2.

mode at this point in the load history. Only a small portion of the damage shows fiber kinking, as marked by the white arrow in the rightmost image of Figure 7. The fibers that kinked have a large misalignment ($\varphi \cong 6°$) whereas the fibers that failed by the shear-driven mode are well aligned. This relationship between fiber misalignment and failure mode is consistent with the explanation provided by Gutkin et al. [5] that shear-driven fiber failure is promoted by large compressive stresses in the absence of fiber rotation. The angle β of the shear-driven fiber damage is ≅45°.

The contrast between the damage observed in the first two kink bands is stark. While K_1 kinked out-of-plane and is accompanied by large delaminations, K_2 developed primarily as shear-driven fiber failure with some in-plane kinking and little delamination. One explanation for the differences in behavior is the lateral constraint on ply 0_1 is much less than ply 0_2, especially if the delamination preceded or was coupled with the kink-band initiation. Due to the sudden formation of K_1, the sequence of kinking and delamination development is unclear. Nonetheless, apparently the kinking plane is related to the lateral constraint on the ply. It also interesting to note that fiber kinking initiation in the outermost 0° ply has been reported previously in the literature [11].

Stage II: Propagation of Initial Kink Bands

During stage II, the two kink bands that initiated in stage I propagated stably and no additional kink bands developed. The evolution of kink band K_1 from scan 30 to 32 is shown in Figure 8. This kink band propagated in both the in-plane direction and out-of-plane direction. Several damage features propagated between these two scans, and apparently the propagation of this damage resulted in the load drop about 50 N, observed in Figure 3. The slices shown in Figure 8a are repeated from Figure 6b with corresponding images from scan 32 shown for comparison in Figure 8b. The distance from the notch tip to the section plane is labeled in white in the upper right corner of each image. The images at a distance of 193 μm and 244 μm from the notch show the delaminations propagating from the kink band have extended and opened. It appears that the ply slides along the kinked interface as the delaminations open. A secondary kink band, marked with white arrows in the images at 244 μm from the notch tip, initiated with large fiber bending and matrix splitting. The fibers within the kink band rotated further from scan 30 to scan 32, as observed in the images at 378 μm, 406 μm, and 427 μm from the notch tip.

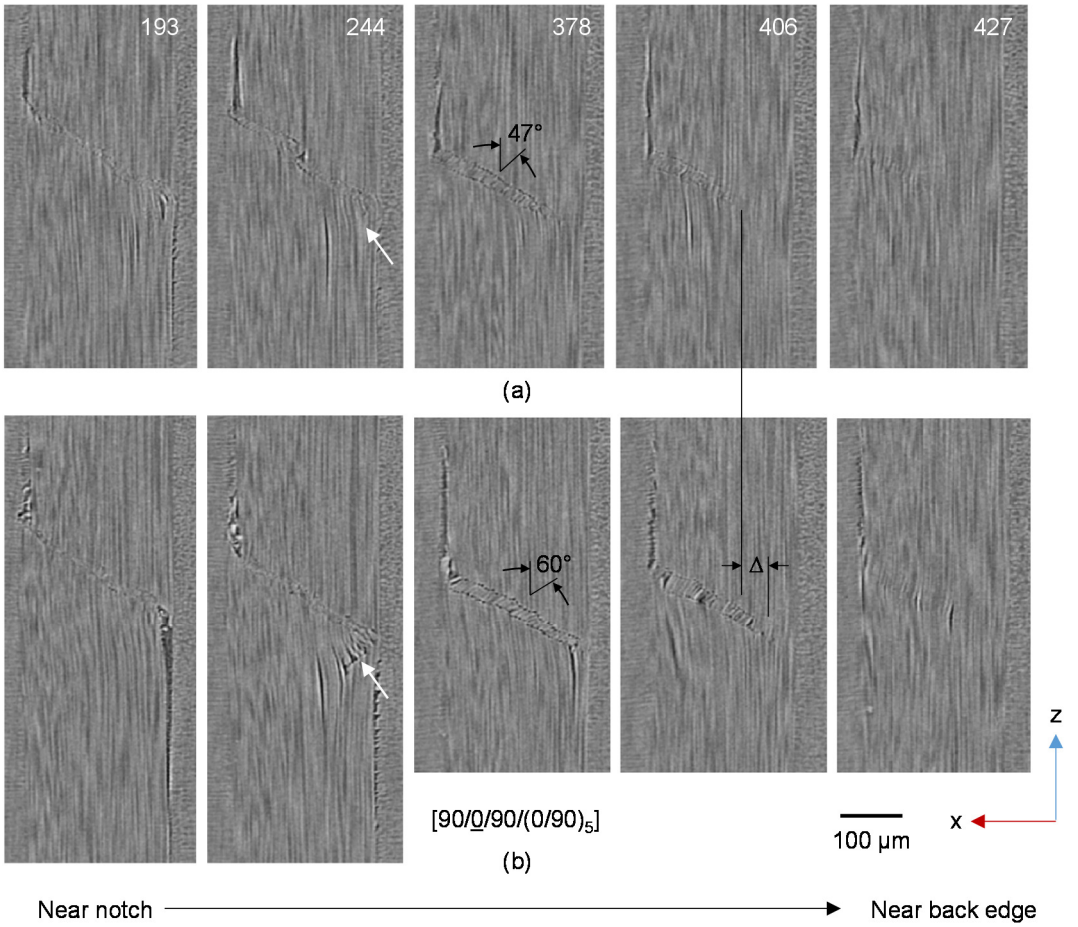

Figure 8. Propagation of kink band K_1: comparison of slices with normal y from (a) scan 30 and (b) scan 32.

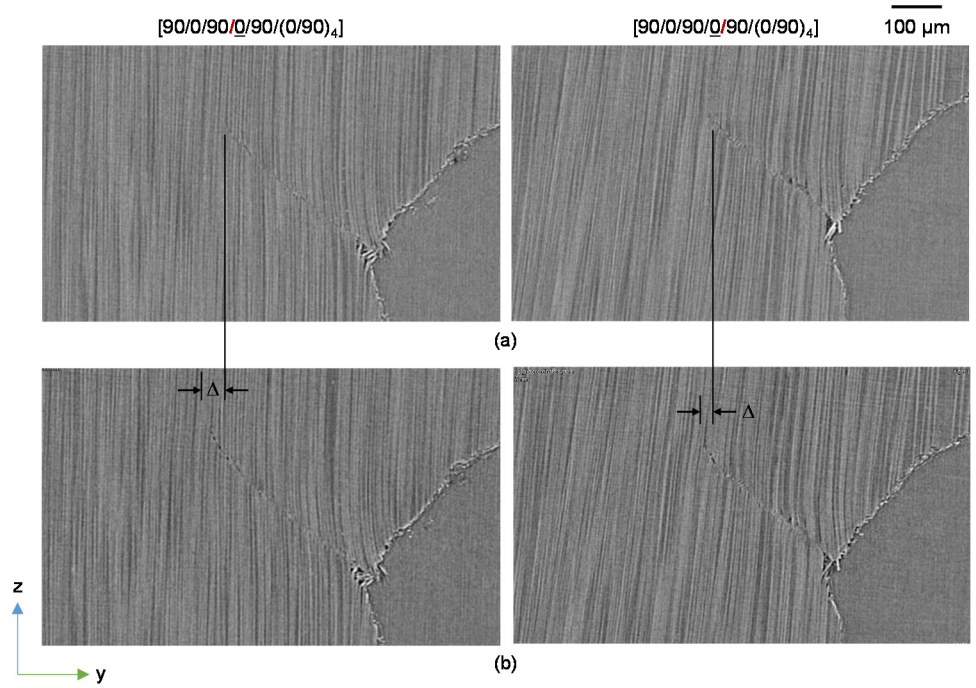

Figure 9. Planar sections showing the propagation of kink band K_2 in (a) scan 31 and (b) scan 35.

Kink band K_2 propagated slowly and stably from scan 31 to scan 35 as shown in Figure 9. Propagation occurred in the in-plane direction by additional shear-driven fiber failure. Examining the variation in propagation through-the-thickness of the ply, it was observed that slightly more propagation occurred near ply 0_1, which is likely related to the damage in ply 0_1.

Stage III: Development of Kink Bands in Remaining 0° Plies

In stage III, kink bands developed in all of the remaining unkinked 0° plies as the load slowly decreased by about 10 N. A cross-section view showing all of the 0° plies and the kink bands at the end of stage III is shown in Figure 10. The kink bands K_3 and K_5 were first observed in scan 36 and the kink bands K_4 and K_6 appeared in the subsequent scan. It is interesting to note that the kinks in the interior plies $K_2 - K_5$ are all in-plane kink bands whereas the kinks in the outermost 0° plies (K_1 and K_6) are out-of-plane kink bands. As was noted previously, apparently the limited lateral constraint of the outermost 0° plies allowed for out-of-plane kinking along with more extensive delamination and matrix splits. It is also observed in Figure 10 that K_1 and K_6 both have secondary kink bands propagated through a portion of the ply thickness (orange arrows). The chronology of the kink band initiation was from left to right in Figure 10 with one exception: K_5 was observed in the scan before K_4. One possible explanation for the sequence of kink band initiations is that kinking of the first ply (0_1) lead to a nonuniform stress distribution. Following this logic, higher stresses in the 0° ply adjacent to the kinked ply precipitated fiber kinking initiation sequentially through-the-thickness of the laminate.

Planar views of the in-plane kink bands (K_3, K_4, and K_5) that developed during stage III are shown in Figure 11. In all cases, there is evidence of shear-driven fiber failure at point where the kink bands initiated (green arrows) and matrix splitting cracks at the notch tip (orange arrows). Kinks K_3 and K_5 occurred in the same location relative to the

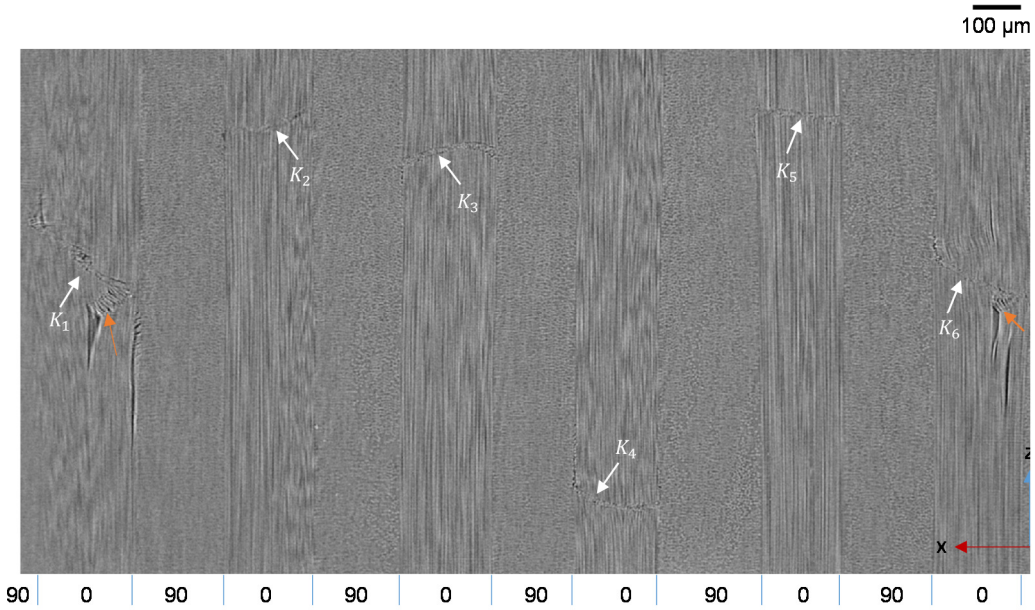

Figure 10. Cross-section showing a kink band in each 0° ply.

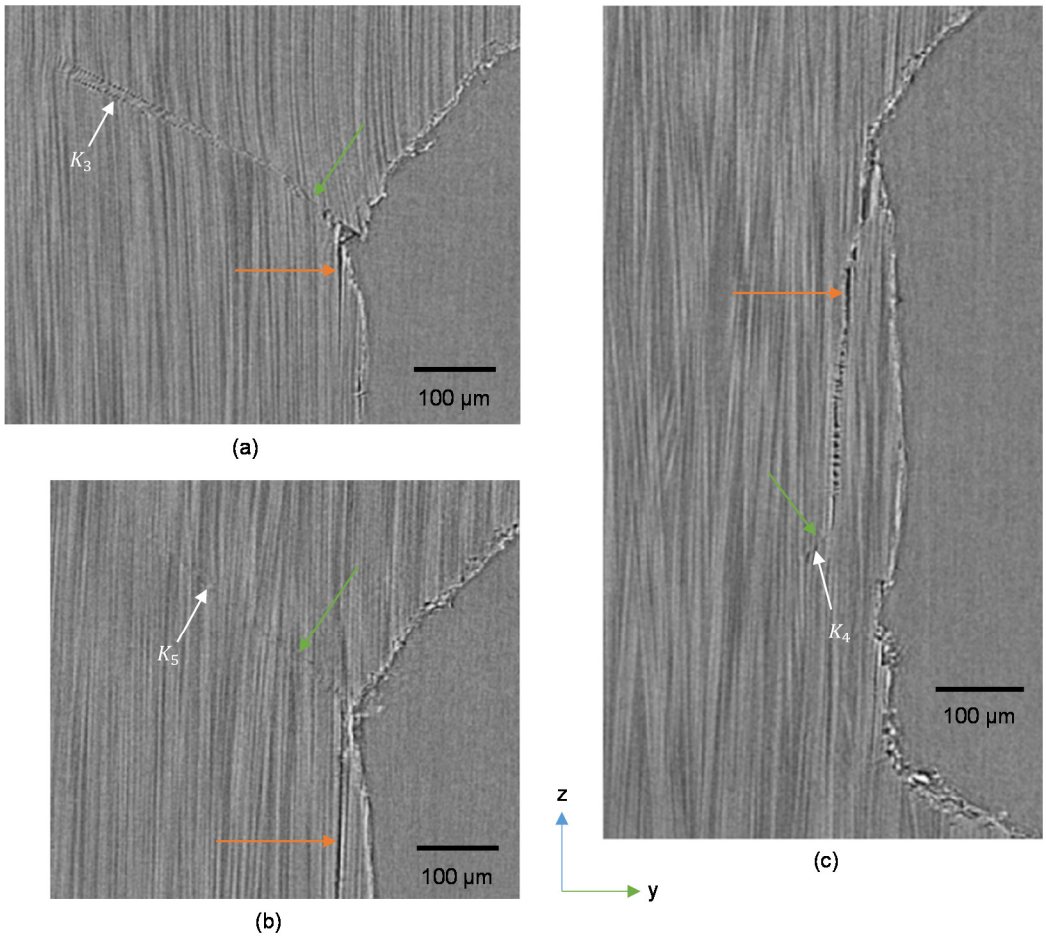

Figure 11. In-plane kink bands that initiated during stage III.

notch as K_2. In contrast, K_4 occurred at the end of a matrix splitting crack. The fact that K_4 occurred at the tip of a splitting crack may explain why it was the last kink to initiate.

Stage IV: Final Collapse

The kink bands propagated slowly and stably from stage II through stage IV, with growth similar as that shown in Figure 8 and Figure 9. In stage IV, transverse compression matrix cracks developed in several of the 90° plies connecting the kink bands and allowing further sliding along the kinked interfaces. The damage continued to grow until nearly the entire ligament ahead of the notch was damaged. Just prior to failure, out-of-plane deformation of the outermost 0° plies is substantial, as shown in Figure 12 where the outermost 0/90 ply interface is traced with an orange line to highlight the deformation in the x-direction. The out-of-plane deformation is a result of secondary kinks, delamination, and longitudinal matrix splitting cracks. The interaction of these damage modes does not allow the sample to maintain its structural integrity and therefore subsequent failure of the specimen occurred.

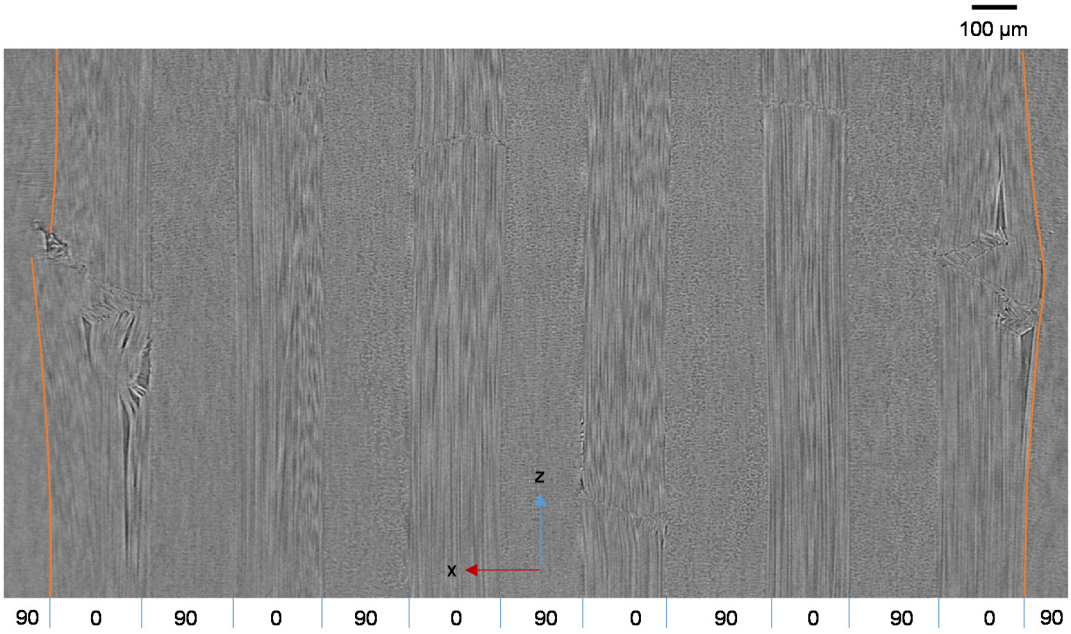

Figure 12. A cross-section view showing the damage just prior to failure.

KINK-BAND MORPHOLOGY

The kink bands observed in the previous section have features varying in three-dimensions. The complexity of the 3-D kink band morphology makes visualization by 2-D cross sectional images difficult. In order to investigate the morphology of kink bands, a segmentation procedure was developed using Matlab [12]. The segmentation procedure and application of the procedure to kink band K_3 in scan 36 are described in this section.

Segmentation Procedure

For the purpose of segmenting a kink band, it is assumed that the bounding surfaces of a kink band can be identified by the fiber breaks above and below the kinked fibers. The steps of the segmentation procedure for identifying the fiber breaks associated with a kink band are shown in Figure 13. The segmentation procedure is applied to a region of interest (ROI) containing a single kink band and it is assumed that the kink is in-plane. A schematic of the kink band and notch (Figure 13a) as observed in the original image (Figure 13b) are shown to orient the reader. The first step of the process is defining a mask loosely around the kinked fibers, shown as a blue overlay in Figure 13c. For each image in the ROI volume, the following steps shown in (d) – (h) of Figure 13 are applied to identify a set of points representing the kink band. The Sobel edge detection filter is applied to identify horizontal edges with a threshold of 0.06 pixel. The result of the edge detection is shown in Figure 13d where the clusters of white pixels indicate locations of detected edges. It can be observed that clusters corresponding to the kink band and notch edge are identified along with some outliers that are not associated with the kinked fibers. One outlier is marked with a blue arrow in Figure 13d. The majority of the outliers can be removed by applying the mask defined in Figure 13c, the result of which is shown in Figure 13e. In the case shown, one outlier remains (see blue arrow in Figure 13e). Outliers such as the one identified in Figure 13e are

filtered from the data by considering the distance to the nearest neighbor. It is assumed that clusters with a large distance to the nearest neighbor are outliers. This filter is applied via dilation followed by thresholding with a minimum cluster area criterion, as shown in parts (f) – (h) of Figure 13. The centroids of the clusters that remain are calculated to generate a set of points associate with the kink band. The points are overlaid on the original image in Figure 13i. Qualitatively, the points represent well the region of the image where the kink band is located. Only a few points are found at locations that a skilled observer would not identify as part of the kink band, in other words, false positives (see blue arrow in Figure 13i). In all cases that were verified manually, less than 1% of points were false positives.

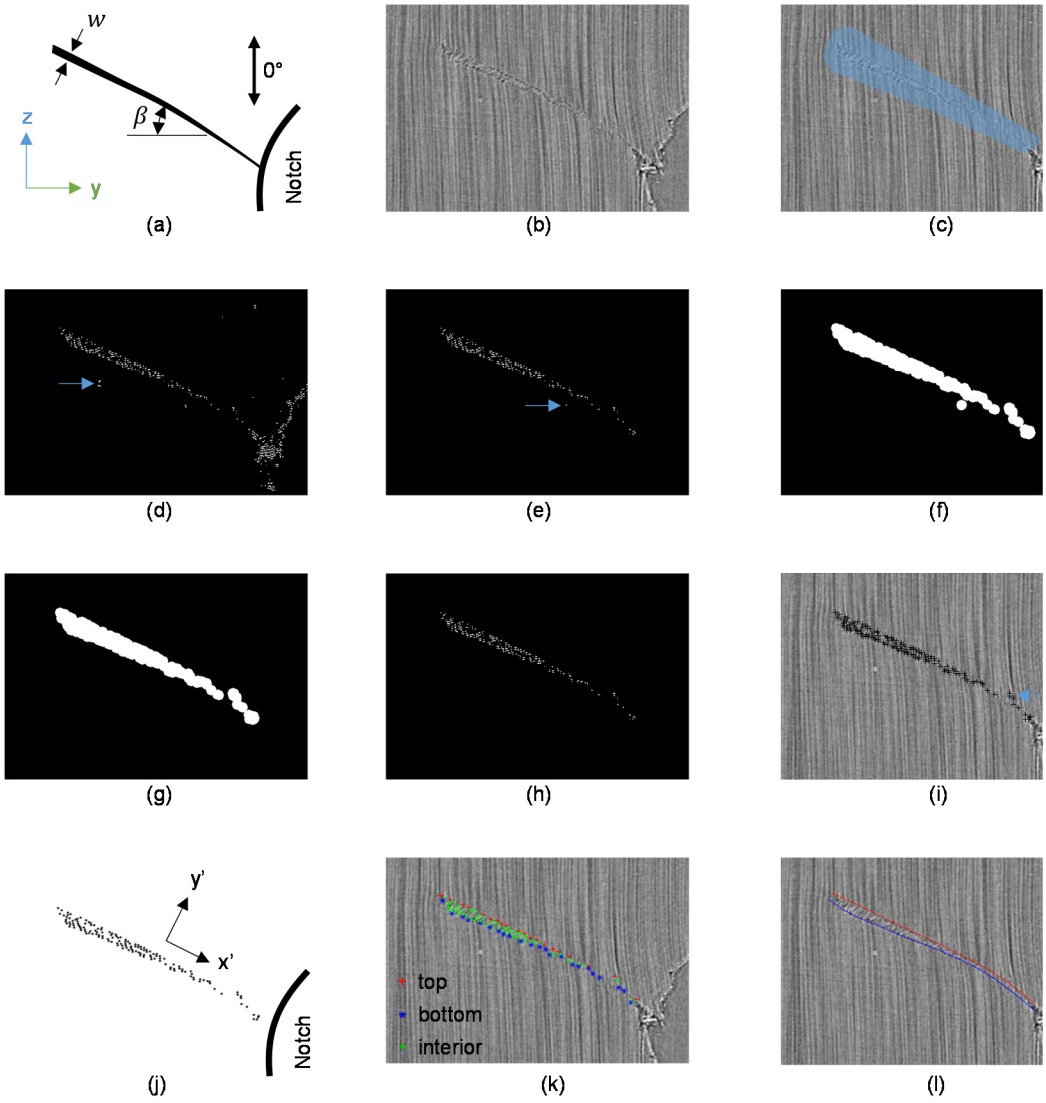

Figure 13. Identification of kink bands: (a) schematic of kink and notch; (b) original image; (c) – (h) steps of the segmentation process; (i) identified points overlaid on the original image; (j) local coordinate system used for point categorization; (k) points identified as top, bottom, or interior relative to the kink band; and (l) a projection of surfaces fit to the kink band boundary points.

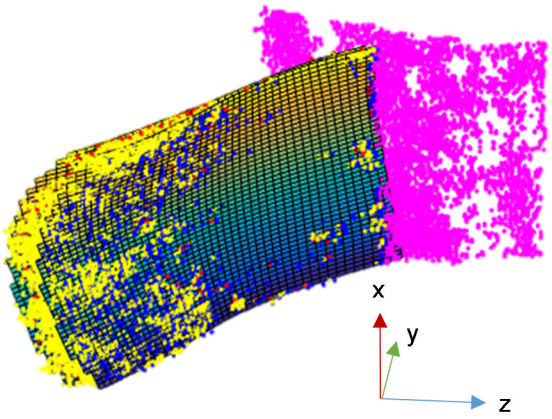

Figure 14. 3-D visualizations of the kink band showing the points identified by segmentation and surfaces fit through the points.

The set of points were further categorized as on the top surface of kink band, on the bottom surface of the kink band, or interior to the kink band as shown in Figure 13j and Figure 13k. The categorization was obtained as follows. A local coordinate system was defined with the x' axis oriented along the length of kink band. Points with a maximum or minimum y' coordinate in a local window in x' are categorized as belonging to the top surface or bottom surface, respectively, and all other points were categorized as interior. The result is shown in Figure 13k, where the red points belong to the top surface of the kink band, the blue points belong to the bottom surface of the kink band, and the yellow points are interior to the kink band. Smooth surfaces are fit to the points belong to the top and bottom boundaries of the kink band. The 2-D projection of these surfaces onto the original image is shown in Figure 13l. It is observed that the fitted surfaces represent accurately the boundaries of the kink bands. In most cases, the difference in position between the broken fibers at the edge of the kink band and the fitted surface was less than one fiber diameter.

The data generated from the segmentation procedure enable 3-D visualization of the kink band, as shown in Figure 14. The notch tip boundary is segmented using a similar procedure and included in the figure for reference (shown as magenta points). The 3-D rendering conveys the orientation, inclination, and spatial variation of the entire kink band in a way that is not possible to reveal using 2-D section views.

Characteristics of a Kink Band in an Interior Ply

The segmented representation allows for quantifying automatically the position of the kink band, the spatial variation of w and β, as well as the length of the kink band. The spatial variation of the kink band inclination angle β is shown in Figure 15. The contour plot represents the region that is kinked where the vertical axis spans through the ply thickness, and the horizontal axis is the projection of the kink band onto the y-axis. The extent of the colored region in the $-y$-direction gives an indication of the length of the kink. It is observed that the kink band tunnels through the ply meaning that the kink has propagated the furthest midway through-the-thickness of the ply while the kink propagation near the ply interfaces is less extensive. The color is mapped to the inclination angle showing larger values of β in the region where shear-driven fiber failure was observed.

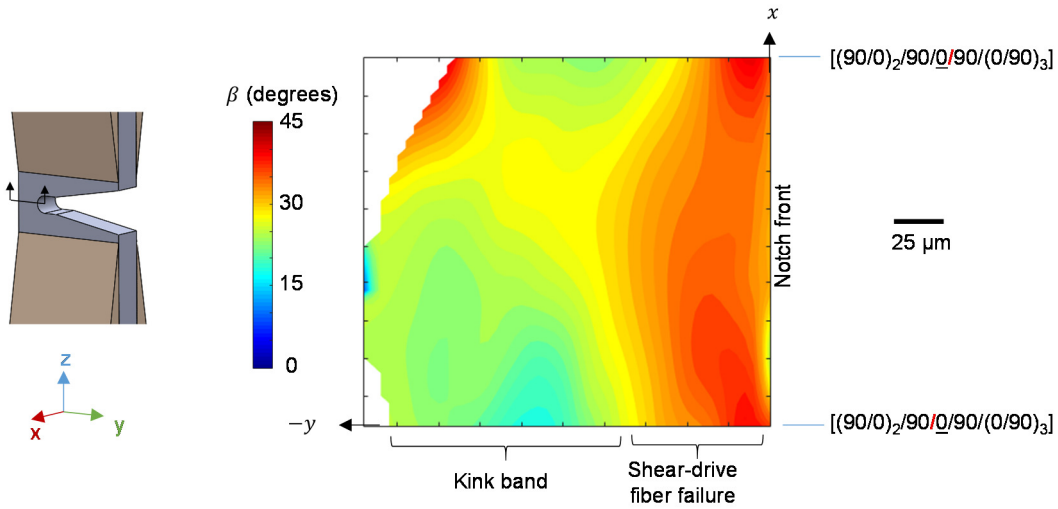

Figure 15. Spatial variation of the kink band inclination angle β of K_3 recorded in scan 36.

SUMMARY

The role of fiber kinking in notched cross-ply laminates was studied experimentally with in-situ synchrotron radiation based computed tomography (SRCT). Carbon/epoxy specimens were loaded quasi-statically in uniaxial compression while recording SRCT scans continuously with a temporal resolutions of 2.4 s and a spatial resolution of 1.1 μm/voxel. The specimens exhibited a quasi-stable failure process that allowed for SRCT observations of damage formation and propagation.

Longitudinal matrix splitting occurred first, with splits developing tangent to the notch tip in most 0° plies. The first kink band initiated in one of the outer-most 0° plies and the fibers kinked out-of-plane. The kink was accompanied by delaminations at both ply interfaces that occurred in locations consistent with the direction of fiber rotation. In the next scan, a second kink band was observed in an interior 0° ply with the fibers kinked in-plane. Out-of-plane kinks were observed in the two outermost 0° plies and in-plane kinks were found in the remaining (interior) 0° plies. One explanation for this pattern of the kinking plane is that lateral constraint on 0° plies is a factor affecting the kinking-plane. Subsequent scans showed evidence of kink band propagation. Load drops appeared to correspond with kink band propagation and not initiation. In all plies, there was evidence that the kink bands initiated with shear-driven fiber failure. Longitudinal matrix splits appeared to be an integral mechanisms in the propagation of the out-of-plane kinks. Secondary kink bands developed in the outermost 0° plies and always initiated at the ply interface in conjunction with delaminations and then propagated with several longitudinal splitting cracks.

An automatic segmentation procedure was developed to identify the kink band boundary surfaces. The segmentation was accomplished using conventional image analysis techniques. Sets of points representing the kink band boundaries were identified and fit with smooth surfaces. This procedure enables 3-D visualization of the kink band and conveys the orientation, inclination, and spatial variation of the kink band, all of which are difficult to interpret from 2-D section views. The kink band inclination and length were examined using the segmented data revealing tunneling and spatial variations not apparent from studying the 2-D sectional data. This segmentation

approach shows promise for further examination of kink band characteristics, variability, and evolution under load.

ACKNOWLEDGEMENTS

The authors would like to acknowledge the Swiss Light Source for access to the TOMCAT-X02DA beamline, and are grateful for the assistance of Dr. Anne Bonnin. Thanks to the INSA-Lyon MATEIS for providing the loading rig used in these experiments and to Dr. Valeriy Titarenko for his support with image reconstructions.

REFERENCES

[1] H. Suemasu, Y. Naito, K. Gozu, and Y. Aoki, "Damage Initiation and Growth in Composite Laminates During Open Hole Compression Tests," *Adv. Compos. Mater.*, vol. 21, no. 3, pp. 209–220, Jun. 2012.

[2] N. Zobeiry, R. Vaziri, and A. Poursartip, "Characterization of Strain-Softening Behavior and Failure Mechanisms of Composites Under Tension and Compression," *Compos. Part Appl. Sci. Manuf.*, vol. 68, pp. 29–41, Jan. 2015.

[3] D. Svensson, K. S. Alfredsson, U. Stigh, and N. E. Jansson, "Measurement of Cohesive Law for Kink-Band Formation in Unidirectional Composite," *Eng. Fract. Mech.*, vol. 151, pp. 1–10, Jan. 2016.

[4] S. T. Pinho, C. G. Dávila, P. P. Camanho, L. Iannucci, and P. Robinson, "Failure Models and Criteria for FRP Under In-Plane or Three-Dimensional Stress States Including Shear Non-linearity," NASA/TM-2005-213530, 2005.

[5] R. Gutkin, S. T. Pinho, P. Robinson, and P. T. Curtis, "On the Transition From Shear-Driven Fibre Compressive Failure to Fibre Kinking in Notched CFRP Laminates Under Longitudinal Compression," *Compos. Sci. Technol.*, vol. 70, no. 8, pp. 1223–1231, Aug. 2010.

[6] M. Ueda, K. Mimura, and T.-K. Jeong, "In Situ Observation of Kink-Band Formation in a Unidirectional Carbon Fiber Reinforced Plastic by X-ray Computed Tomography Imaging," *Adv. Compos. Mater.*, vol. 25, no. 1, pp. 31–43, Jan. 2016.

[7] Y. Wang, T. L. Burnett, Y. Chai, C. Soutis, P. J. Hogg, and P. J. Withers, "X-ray Computed Tomography Study of Kink Bands in Unidirectional Composites," *Compos. Struct.*, vol. 160, pp. 917–924, 2017.

[8] Y. Wang, C. Soutis, and P. J. Withers, "Time-Lapse X-ray Microtomographic Imaging of Compressive Failure in Carbon Fibre-Epoxy Composites," presented at the 20th International Conference on Composite Materials, Copenhagen, Denmark, 2015.

[9] E. Maire, C. L. Bourlot, J. Adrien, A. Mortensen, and R. Mokso, "20 Hz X-ray Tomography During an In Situ Tensile Test," *Int. J. Fract.*, vol. 200, no. 1–2, pp. 3–12, Jul. 2016.

[10] T. Fast, A. E. Scott, H. A. Bale, and B. N. Cox, "Topological and Euclidean Metrics Reveal Spatially Nonuniform Structure in the Entanglement of Stochastic Fiber Bundles," *J. Mater. Sci.*, vol. 50, no. 6, pp. 2370–2398, Mar. 2015.

[11] C. Soutis, N. A. Fleck, and P. A. Smith, "Failure Prediction Technique for Compression Loaded Carbon Fibre-Epoxy Laminate with Open Holes," *J. Compos. Mater.*, vol. 25, no. 11, pp. 1476–1498, Nov. 1991.

[12] "MATLAB 2015a, The MathWorks Inc.," Natick, MA, 2015.